

Supplementary Information:

Anomalous Impact and Strain Responses in Helical Carbon Nanotube Foams

Ramathasan Thevamaran^{1,2}, Mehmet Karakaya³, Eric R. Meshot⁴, Andre
Fischer², Ramakrishna Podila³, Apparao M. Rao³, Chiara Daraio^{1,2,*}

¹*Division of Engineering and Applied Sciences, California Institute of Technology, Pasadena, CA
91125, USA.*

²*Department of Mechanical and Process Engineering, Swiss Federal Institute of Technology
Zurich (ETH Zurich), Zurich 8092, Switzerland.*

³*Department of Physics and Astronomy, and Clemson Nanomaterials Center, Clemson
University, Clemson, South Carolina 29634, USA.*

⁴*Physical and Life Sciences Directorate, Lawrence Livermore National Laboratory, Livermore,
CA, USA.*

**Corresponding author: daraio@ethz.ch*

[S1] Intrinsic density and alignment characterization methods.

We performed synchrotron X-ray scattering and mass attenuation measurements to nondestructively quantify the density and alignment within HCNT foams. A beam energy of 10 keV was selected with a Mo/B₄C double multilayer monochromator, and the height of the beamspot was less than 300 μm at the sample with a measured flux of 10¹² photons sec⁻¹. The HCNT sample was mounted on a motorized stage that enables 1) tilt alignment to make the sample's Si substrate parallel to the X-ray beam as well as 2) spatial mapping of the structural characteristics of the sample along its height.

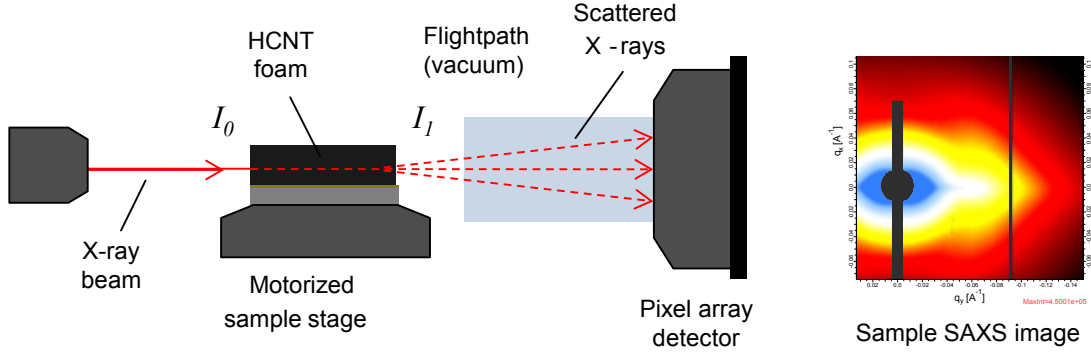


Figure S1(a): Schematic side view of the experimental setup for X-ray characterization with a representative SAXS image collected from our HCNT foams. The x-z-α stage enables spatial mapping and alignment of the HCNT to the X-ray beam, and the scattered X-rays are collected on a Pilatus 1M pixel detector.

We monitored the X-ray intensity upstream (I_0) and downstream (I_1) of the sample by measuring ion current at the locations denoted in the schematic. These values were used to calculate the mass density of the sample based on the Beer-Lambert law [1],

$$\rho_{\text{CNT}} = \frac{\ln(I_0/I_1)}{t(\mu/\rho)},$$

where ρ_{CNT} is the HCNT volumetric mass density, t is the path-length through the HCNT, and (μ/ρ) is the mass attenuation coefficient. Values for (μ/ρ) are tabulated by NIST as a function of element and X-ray energy [2].

In addition to measuring the X-ray attenuation, we also quantified the average CNT alignment from the anisotropy of small-angle X-ray scattering (SAXS) patterns. Using the distribution of scattered intensity about the azimuthal angle ϕ , we calculated the Hermans orientation factor [3,4],

$$f = \frac{1}{2}(3\langle \cos^2 \phi \rangle - 1).$$

Here, f equals 1 for perfectly aligned CNTs and 0 for random order (no alignment), and

$$\langle \cos^2 \phi \rangle = \frac{\int_0^{\pi/2} d\phi I(\phi) \sin \phi \cos^2 \phi}{\int_0^{\pi/2} d\phi I(\phi) \sin \phi}.$$

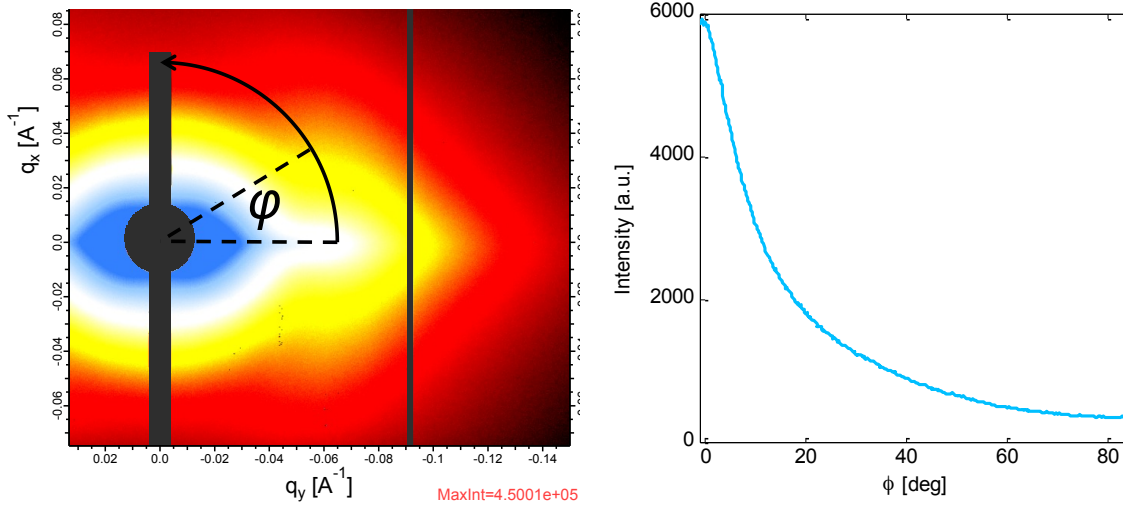


Figure S1(b): Schematic illustration that demonstrates the azimuthal integration we perform on SAXS images to extract the Herman’s orientation factor. The annulus of the azimuthal scan about ϕ is defined by ± 5 pixels from the CNT form factor scattering peak located near $q = 0.05$ - 0.07 \AA^{-1} . We only use one half of the SAXS image because HCNT alignment is isotropic in the plane of the catalyst substrate (Si), so the SAXS pattern is vertically symmetric.

[S2] Loading history dependency in quasistatic compression cycles.

The measured peak stresses during five consecutive loading cycles are shown in Fig.S2 below. The peak stress decreases rapidly within the first three loading cycle and remains nearly constant for the later cycles. This implies that the compressive strength of HCNT foams is loading history dependent.

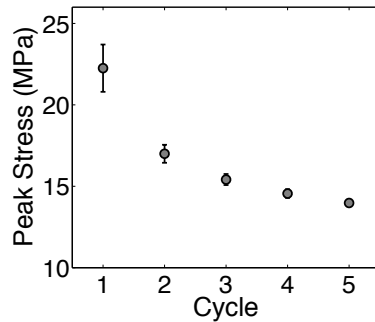


Fig.S2: Decrease in peak stress with compression cycles.

[S3] Deformation mechanisms during a quasistatic compression cycle: HCNT foams.

We performed a quasistatic compression cycle on a pristine (as-grown) HCNT foam sample while obtaining SEM images at different compression levels (Fig. S3(a)). When the sample was compressed strain localized at the bottom low-density region first and then the external free-boundary underwent brittle fracture. The fractured boundaries impede the view of internal sections of the sample. Therefore, we performed another experiment where we first quasistatically compressed an HCNT foam sample on the *Instron* compression testing system and then performed a second compression cycle on the sample inside an SEM, after removing fractured edges (Fig. S3(b)). This allowed us to view the characteristic deformation mechanisms of the bulk sample. The SEM image sequences corresponding to these compression experiments are given below.

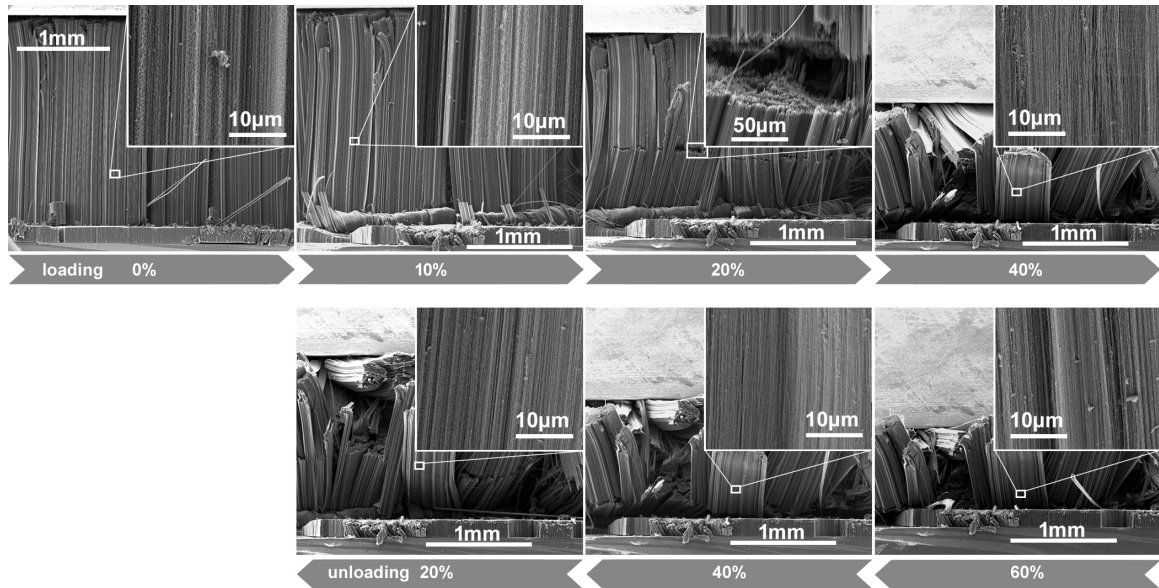


Fig. S3(a): SEM image sequence of a pristine (as-grown) HCNT foam sample under a quasistatic compression cycle up to 60% compression. Insets show magnified views of the regions indicated by the boxes in the large images. Structural buckle formation at the bottom low-density region and the bundle fracturing upon further compression are observable in the images.

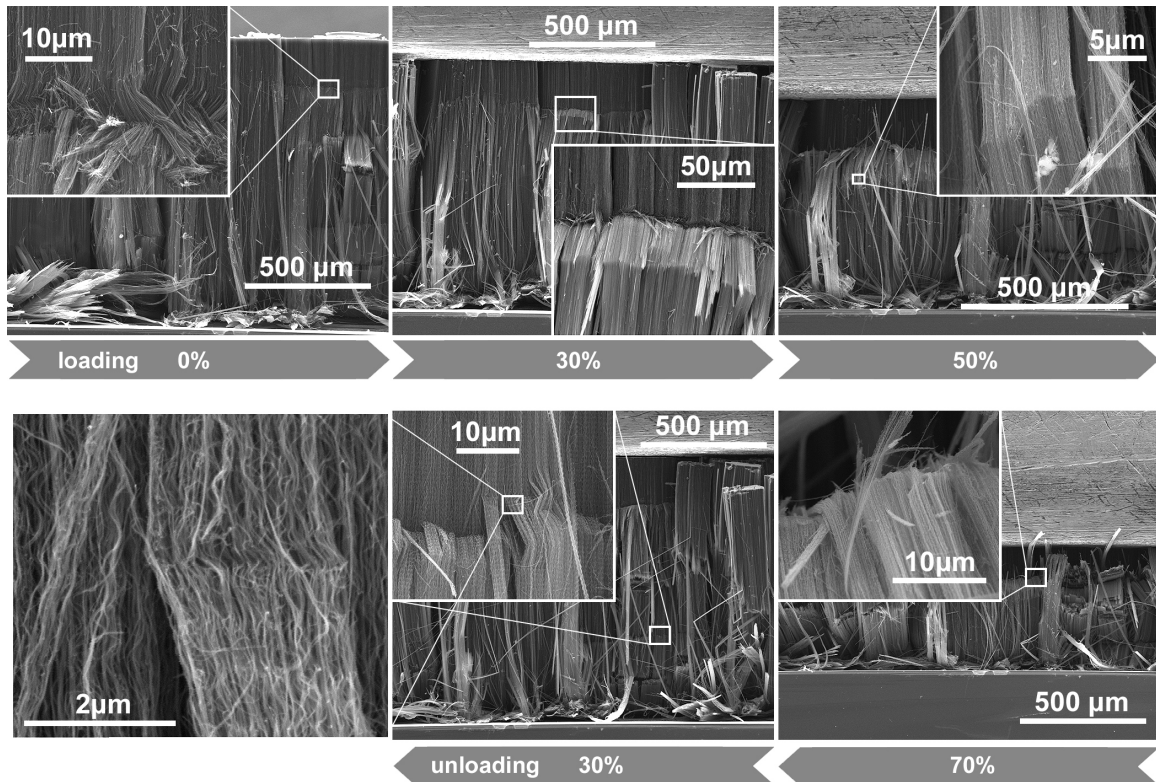


Fig. S3(b): SEM image sequence of an HCNT foam sample under quasistatic compression cycle (second cycle) up to 70% strain. Insets show magnified views of the regions indicated by the boxes in the large images. Structural buckle formation and the buckle induced microstructural changes are observable in the images. The bulk sample shows significant recovery upon unloading with traces of the deformation history in the micro-scale. These SEM images were obtained as follows: first a HCNT foam sample was compressed on the *Instron* compressing testing system up to 80% strain; then the edges of the recovered sample was cutoff to remove fractured external edges to view internal section of the sample; finally, the sample was subjected to a quasistatic loading-unloading cycle in a custom-made vice to perform SEM at different compressive strains.

[S4] Deformation mechanisms during a quasistatic compression cycle: VACNT foams.

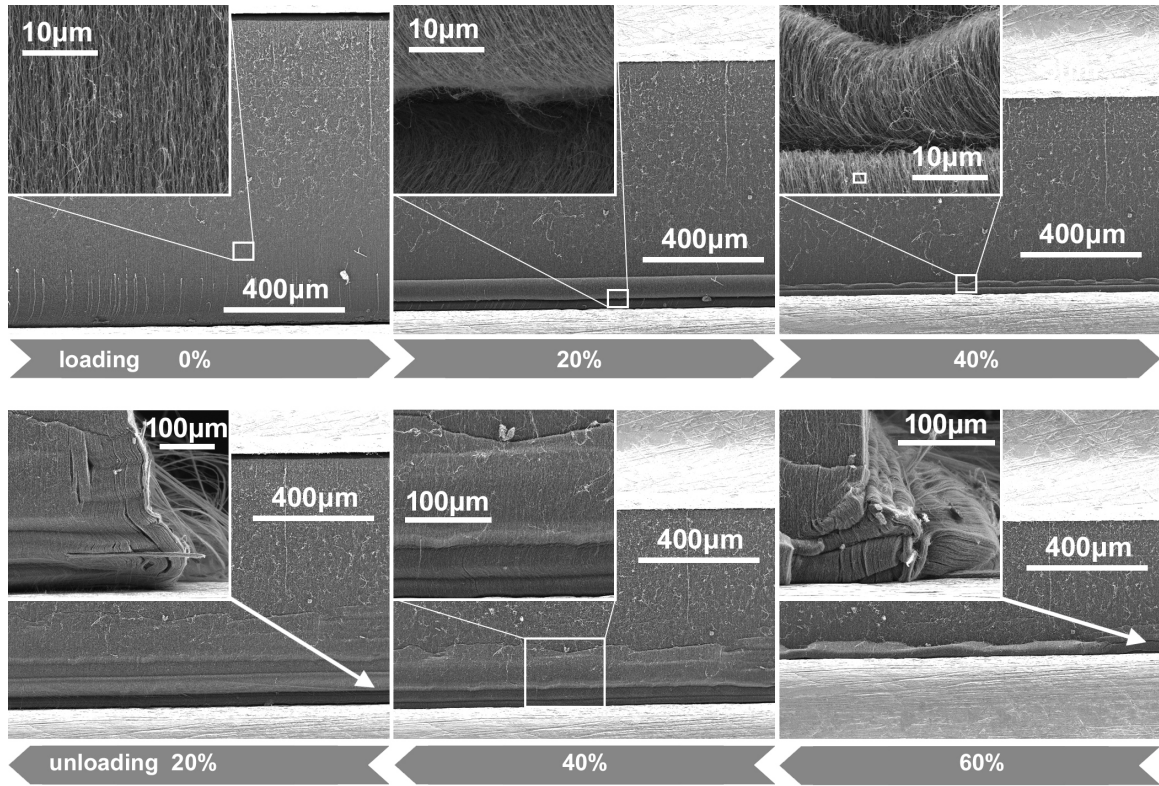


Fig. S4: SEM image sequence of a pristine (as-grown) VACNT foam subjected to a quasistatic compression cycle up to 60% strain. The collective buckle formation and sequential progression of the buckles from the bottom soft region towards upper stiffer region can be seen on the images. The samples show a significant recovery upon unloading. The SEM at different compressive strains was performed while quasistatically compressing the sample in a custom-made vice.

[S5] Comparison of dynamic responses of HCNT foams and VACNT foams.

Dynamic responses of HCNT foams in comparison to that of the VACNT foams with similar densities and thicknesses are presented in Fig.S5. Both CNT foams exhibit similar dynamic cushion factor (Fig.S5(a)), but the HCNT foams damp the transmitted impact stress amplitude more efficiently compared to the VACNT foams (Fig.S5(c)). VACNT foams exhibit higher hysteresis energy dissipation (Fig.S5(b)) due to the higher peak stresses reached during impact, forming large hysteresis area.

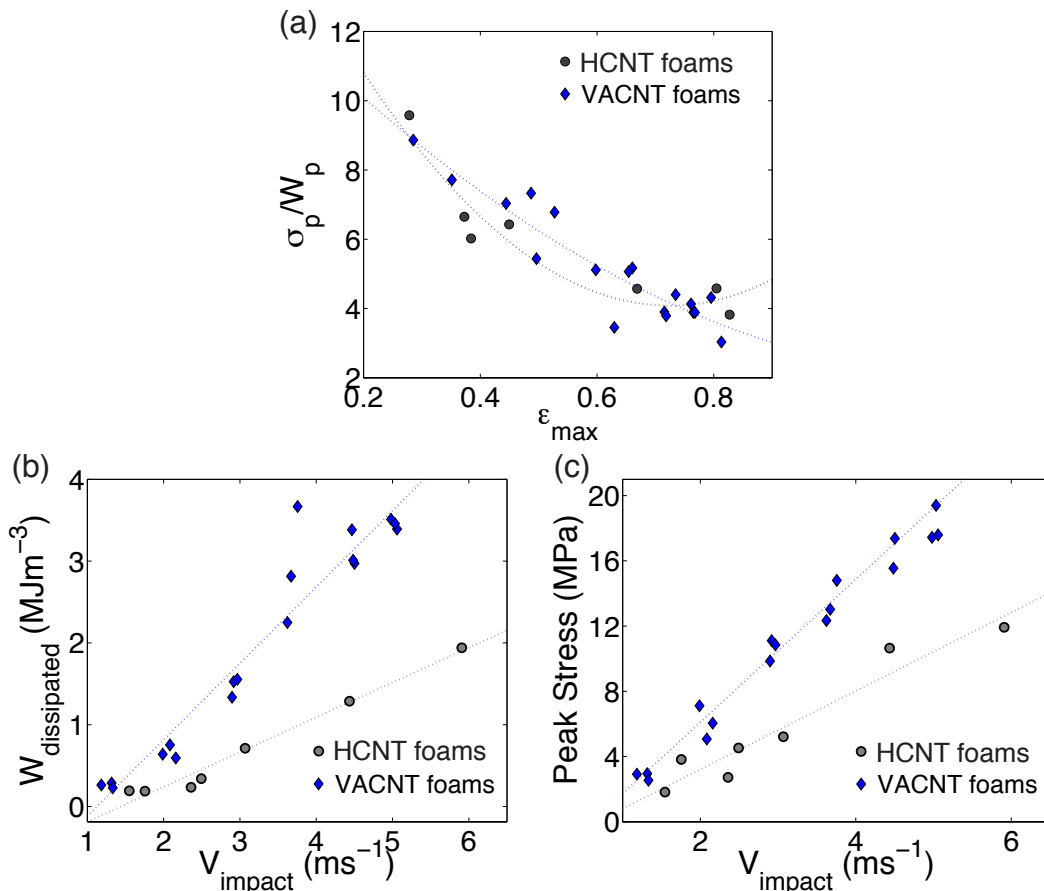


Fig. S5: (a) Dynamic cushion factor with maximum strain reached on impact, (b) hysteretic energy dissipation with impact velocity, and (c) peak stress with impact velocity.

References

- [1] Bedewy M, Meshot ER, Reinker MJ, Hart AJ. Population growth dynamics of carbon nanotubes. ACS Nano 2011;5:8974–89.
- [2] <http://physics.nist.gov/PhysRefData/XrayMassCoef/ElemTab/z06.html>.
- [3] Meshot ER, Hart AJ. Abrupt self-termination of vertically aligned carbon nanotube growth. Appl Phys Lett 2008;92:-.
- [4] Wang B, Bennett R. Quantitative characterization of the morphology of multiwall carbon nanotube films by small angle X-ray scattering. J Phys Chem C 2007:5859–65.